

Ballistic study of Tensylon[®]–based panels

L–C. Alil¹, M. Arrigoni², S. Badea³, R. Ginghină³, L–C. Matache³, P. Mostovkykh^{2*}

¹Doctoral School ‘Engineering of Systems for Defense and Security’, Military Technical Academy, 39–49 George Coșbuc Avenue, 050141 Bucharest, Romania

²IRDL FRE CNRS n° 3744, ENSTA Bretagne, 2 rue François Verny, 29806 Brest, France

³Scientific Center for CBRN Defence and Ecology, 225 Olteniței, Bucharest, Romania

Received 17 October 2017; accepted in revised form 16 January 2018

Abstract. Ballistic protection is a matter of interest requested by civilian as well as military needs. The last decade has witnessed an increase in the use of light weight and efficient armour systems. These panels may be used for body protection as well as light vehicle protection against small calibres or to enhance the protection level of heavier vehicles with decreasing or maintaining their weight penalty. Ultra high molecular weight polyethylene is a material of interest for light weight armour applications. The authors designed panels made of hot–pressed Tensylon[®] in different configurations with thin steel sheets as a backing and shield protection. Comparison of their ballistic performance to the theory predictions reveals the improved ballistic response of the panels. In addition, a non–pressed Tensylon[®] panel has been tested in order to facilitate the observations of the failure mechanisms inside the panels. Even if not suitable for practical use, such non–pressed panels clearly reveal the dynamic processes at micro–scale that occur during the impact. The failure mechanisms of the material under bullet penetration are discussed based on photography, optical microscopy and scanning electron microscopy. The supposed effects of the panel pressing are discussed based on the observed difference between pressed and non–pressed structures ballistic response.

Keywords: *polymer composites, failure mechanism, criss–cross composites, Tensylon[®], ballistic testing*

1. Introduction

Different failure mechanisms under bullet penetration occurring in high–modulus high–strength polymeric materials have been revealed in the literature. These mechanisms have been phenomenologically described in several papers such as [1] and [2], and have been highlighted in photographs by various authors, including [3, 4]. These mechanisms include cutting of the material fibres or filaments (also known as ‘punching’ [1]), stretching accompanied by deflection of the panel, friction between the bullet and its surrounding, energy transfer by the waves away from the impact, etc. Except for friction, in all these mechanisms the fibre tension contributes substantially to the bullet stopping, and therefore the fibre rupture in tension plays a determining role in allowing the bullet

to perforate. The model of Cunniff [5], especially, assumes that it is the only mechanism acting, whereas Walker [6] considers, in addition, the effect of the material shear strength resulting in shear waves propagation.

It should be noted that Cunniff’s mechanism supposes a significant back face deformation (BFD) of a protective panel. In other words, the possibility of deformation at the back of the ballistic panel appears as a prerequisite for efficient protection against a bullet. This was understood as a high V_{50} velocity, i.e. the critical velocity with which 50% of the projectiles perforate the panel, given a protective panel with a specific areal density, at the impact with a specific projectile. However, a high V_{50} velocity is not the only requirement for individual ballistic armour: the BFD,

*Corresponding author, e-mail: mostovkykh@gmail.com
© BME-PT

approximately equivalent to the back face signature (BFS) in a modelling clay backing material, is specified in [7]. In order to decrease the BFD, a variety of ballistic panel modifications have been proposed, the simplest being the use of thicker panels and the use of a layer of material with higher bending stiffness in combination with a polymeric panel. Numerous experimental studies [1, 8, 9] evidence that thick composite panels deform in stages, with partial penetration as a possible test output. In this case, a cavity containing both the deformed bullet and the debris of the protective panel is found in the post-mortem analysis of the ballistic panels. The Cunniff's ballistic response mechanism, and the Cunniff velocity [5] as a measure of ballistic performance based on it, which consider only two possible results of a ballistic test – no penetration and full penetration –, are, therefore, insufficient. Analogous considerations apply to stratified ballistic solutions as well.

Frissen [1] suggests that the cavity appears around the panel mid-plane. The theoretical explanation of this assumption is nevertheless debatable. Indeed, the out-of-plane shear stresses are maximum in the mid-plane under quasi-static bending of isotropic media, but the impact process is far quicker to establish the characteristic bending stress profile. In addition, experiments [10] on Ultra-High Molecular Weight PolyEthylene (UHMWPE) bending has shown that kinking under compression (on the side of the panel loaded in compression along the fibres, i.e. in-plane) usually occurs at a lower stress than delamination on the mid-plane. We were, therefore, interested in experimental verification of the cavity location in the panel thickness under various conditions. In this study, several configurations of ballistic panels made of Tensylon® (simple and in combination with a thin steel sheet), have been subjected to ballistic testing with 7.62 mm calibre bullets, a common threat in operation theatres. The residual deformation of the panels tested was qualitatively assessed, and the bullet penetration and damage mechanisms were discussed. Post-mortem visual, microscopic and SEM analysis allowed to determine the overall deformation pattern during the panel-bullet interaction.

Post-mortem analysis of the interior of ballistic panels usually requires intrusive methods, presumably cutting and often polishing in order to facilitate microscopic observation. However, highly anisotropic polymeric materials like UHMWPE are known to be difficult in machining like cutting. It complicates the

possibility of post-mortem analysis. In order to facilitate its optical microscopy and SEM analysis, ballistic impact into a non-pressed panel of Tensylon® (i.e., a sequence of ply-precursor tapes of Tensylon® obtained directly from the manufacturer) was fulfilled. The penetration and damage mechanisms were then clearly visualised since the post-mortem pictures clearly reveal the dynamic processes that had occurred. Due to significantly inferior ballistic performance (compared to pressed Tensylon® panels of the same weight), bigger thicknesses and problems with handling, non-pressed panels are not suitable for practical use. Nevertheless, the visualized mechanisms of the bullet penetration like tape tension until failure, inter-ply delamination are characteristic for the material in the hard (i.e. pressed) panels, too (while other penetration mechanisms, like shear wave propagation in the panel, occur in the hard panels only). Comparison of the non-pressed and pressed panels response gives an estimate of each of the mechanisms role in the overall performance.

This article is organised as follows. After a review of the open literature given in section 1, the description of the materials used and the experimental set-up is given in section 2. Results obtained on non-pressed Tensylon® panels are given in subsection 3.1 and their comparison with the performance of a fully pressed Tensylon® panel in bare and steel-supported protective solutions is presented in subsection 3.2.

2. Experimental configurations and testing procedure

2.1. Materials description

Tensylon® is a trademark of UHMWPE manufactured by the DuPont™ company (better known for commercializing aramid Kevlar® fibres). This product is primarily proposed for ballistic protection applications for lightweight personal armour as well as a component in vehicle protection systems. The Tensylon® panels used in the experiments were manufactured by S.C. STIMPEX S.A. in Bucharest, Romania. The hydraulic presses available are manually controlled and the hard polyethylene panels are typically obtained by the procedure described in Table 1.

In order to cover a large range of usage, several panel dimensions have been used. Larger dimensions (500×500 mm) are characteristic for shield products used, for instance, in vehicles, whereas the 250×300 mm panels are common as inserts in the ballistic vests for personal protection. Since the panels

Table 1. Pressing stages for Tensylon® hard ballistic plates.

Stage	Pressure [MPa]	Temperature [°C]	Duration [min]
1	4.1	60	15
2	8.1	100	45
3	15.2	120	90
Cooling	–	120→30	30/overnight

are considered both for individual and collective ballistic protection applications, both separate and stratified solutions with steel protection sheets placed in front (shield) or on the back (backing) of the UHMW-PE panel were tested. In addition, a 300×300 mm non-pressed structure, screw-fixed in a steel frame, has been tested under the same conditions. The tested protective solutions characteristics are summarized in Table 2.

The thickness of a thin steel sheet in all the panels tested is, if isolated, an insufficient ballistic protection means. For instance, using the data of [11] in the Cunniff parameter scaling approximation, we have found that, in order to defeat the threat used in the present experiments, an 8 mm steel sheet is required, whose areal density is 62 kg/m². For comparison, the bare Tensylon® panel tested is approximately 21 kg/m², a Tensylon® plate with a 2.5 mm or 3 mm thick steel front/back protection is 40 kg/m², respectively 44 kg/m², a Tensylon® plate sandwiched between 2.5 mm thick steel sheets is 60 kg/m², whereas the sandwich version with 3.0 mm thick steel sheets would be 67 kg/m².

All the tested samples contained the same number of Tensylon® pre-preg layers – 196, and since each layer of Tensylon® consists of two unidirectional plies, it corresponds to 392 plies. The pressed panels linear dimensions are defined with 0.5 mm accuracy (as the sides of the panels are uneven, and the front and back faces are not ideally planar, nor parallel to each other). The non-pressed panel thickness strongly depends on the force used by the micrometer to measure it; the corresponding value is reported for reference only.

2.2. Test configuration and procedure

The experiments were performed in the Shooting Range for Experimental and Reception Activities within the Scientific Research Center for CBRN Defence and Ecology of the Romanian Ministry of Defence. The testing configuration was set according to the Romanian standard STM 40202-99, and the internal procedure PO-02512C-14.00-017, in agreement with the NIJ standards [12, 13]. The panels were clamped to the shooting support from two sides, with the longer side up. All the panels were subjected to the impact of the AKM (Kalashnikov) 7.62×39 mm full metal jacket/lead core (FMJ/LC) bullets. The geometrical and mechanical properties of these bullets are similar to [14]. The bullets were fired from a distance of 10.0±0.1 m at normal incidence to the target. The bullet velocity was measured using the Oehler chronograph (model 43); its three screens were placed 1, 1.5 and 2 m away from the muzzle. The measured velocity value, given in Table 3, is, therefore, a bit higher than the impact velocity. Their difference can be estimated by comparison of the bullet kinetic energy $m_p V^2/2 \approx 2$ kJ and the work that the air resistance to the bullet makes during its flight $C_d \rho A_p V^2 L/2$. For the bullet mass m_p , cross-section A_p and initial velocity V of interest, $L = 10$ m of flight with the drag coefficient C_d of unity would result in 130 J of energy loss, i.e. in 3% of velocity loss (here ρ is the air density). Since the drag coefficient for an aerodynamically profiled bullet is lower, the actual velocity overestimate will be below 3%. Two strikes were performed on each of the panels 2 to 5, and five strikes were performed on panel 1, according to their dimensions.

The experimental parameters of the bullet (its mass, calibre and striking velocity) and the protection material characteristics are most readily comparable on the ‘Cunniff plane’. This plane depicts the striking velocity (dimensional or scaled with the Cunniff velocity) vs the nondimensional Cunniff parameter, characterizing the shooting conditions. This parameter is

Table 2. Shooting conditions for the panels tested.

Panel [n°.]	Pressed	Dimensions [mm]	Initial mass [g]	Bulk density [g/cm ³]	Front/back protection characteristics
1	+	500×500×22.5	5300	0.94	2.5 mm magnesium based steel sheets – front and back
2	+	250×300×22.5	1580	0.94	No
3	+	250×300×22.5	1610	0.95	3.0 mm magnesium based steel sheet – front
4	+	250×300×22.5	1600	0.95	3.0 mm magnesium based steel sheet – back
5	–	300×300×27.0	1920	–	No

the protective panel areal density (AD in kg/m^2) normalized with the bullet mass m_p and the characteristic cross-sectional area A_p . The ‘Cunniff plane’ is material-specific, and can be used to predict the ballistic performance (V_0 , V_{50} , etc) against one threat if its performance against other threats is known. In addition, the semi-empirical models [6, 8, 15] predict the V_{50} value based on the material quasi-static properties, such as its Young modulus, shear strength, longitudinal strain to failure, and the material composition (proposed for fibrous materials, the fibre fraction was introduced in the modelling). Since the ‘fibre fraction’ is unavailable for Tensylon[®], we used the values for a similar UHMWPE product, Dyneema[®] HB26, with supposedly similar ballistic properties, as proposed in [8]. They are: the ‘fibre fraction’ of 83%, ‘fibre modulus’ of 131 GPa and the strain to failure of 0.02. The resulting ‘Cunniff plane’ for Tensylon[®] is presented on Figure 1. Thus, the areal density of the Tensylon[®] hard ballistic panel for the ballistic experiments was chosen so that the testing conditions corresponded to the V_{50} value as predicted by the model of [8]. It should be noted that the type of bullet used is different (we used FMJ/LC whereas [8, 9] used fragment simulating projectiles (FSP) of calibres 5.56, 12.7 and 20 mm), and the theory predictions at high velocities differ considerably, as can be seen on Figure 1. Since the theory of [8] is semi-empirical based on FSP bullets, and the two materials differ in their manufacturing process, the model

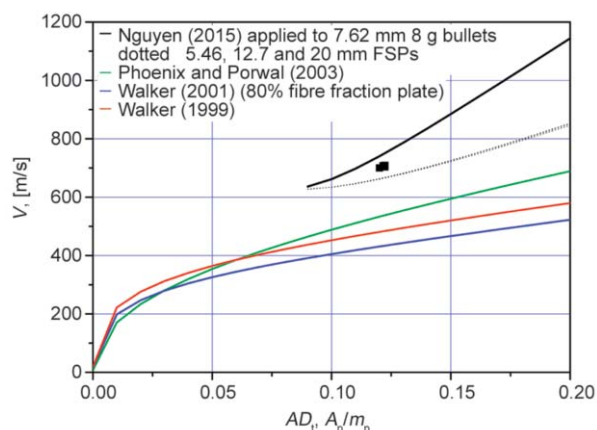


Figure 1. The ballistic experiments fulfilled in the impact velocity-scaled ballistic panel areal density (‘Cunniff’) plane. The dots represent the shooting conditions chosen by the authors for the panels 2 and 5.

of [8] provides us with only a rough estimate for the test conditions.

The test parameters achieved (locations of impacts, bullet speed), as well as the preliminary visual observations of the impacted panels, are given in Table 3. The origin for the cartesian system on each panel was its upper left corner, facing the bullet entrance, so that the axes were directed to the right and downwards, respectively.

In order to observe the internal structure of the impact and penetration-induced holes, the panels were water-jet cross-sectioned through the impact axis along their thickness and one of the two tape main directions. Two samples holes (one from panel 2 and

Table 3. Impact velocities and post-mortem observations (before water-jet cutting).

Panel [n°.]	Shot [n°.]	Initial velocity [m/s]	Coordinates [mm, mm]	Observations
1	1	701	[162, 138]	distances between the impact holes 1–2: 181 2–4: 179 1–4: 139 3–5: 188 2–3: 134 4–5: 96
	2	697	[116, 324]	
	3	703	[250, 426]	
	4	699	[301, 178]	
	5	693	[397, 240]	
2	1	~700	[78, 72]	• distance between the impact holes: 187 mm • partial penetration • wide deflection on the back side (~42.5 mm circumference of the bulge)
	2	~700	[182, 230]	
3	1	709	[143, 63]	• distance between the impact holes: 113 mm • small deflection on the back face • melting is observed around the area where the shield steel sheet has interfered with the bullet • bullet didn’t interact with the UHMWPE panel directly
	2	703	[112, 172]	
4	1	708	[161, 121]	• distance between the impact holes: 80 mm • partial penetration • the backing steel sheet also suffered a deflection
	2	706	[101, 172]	
5	1	688	[102, 195]	• distance between the impact holes: 136 mm • complete penetration
	2	703	[243, 116]	

one from panel 4) were previously filled with clear resin to maintain the position of the material debris and fibrils. The remaining holes in these panels, as well as the holes in panels 3 and 1 (including the protection steel sheets), were waterjet sectioned without applying resin. The *Resato R-LCM 3815-1* cutting table was used, the cuts were performed from the front side of the panels using a low-force gripping of them. Even if the least destructive, (compared to disk cutting, for instance, as evidenced in [16]), the waterjet cutting is still an intrusive technique. Therefore, the imaging of the internal structure without application of resin resulted in fuzzier pictures (probably, due to micro-oscillations under optical observation). The application of resin preserved the initial position of ruptured elements and bullet fragments, allowing for clear images even without additional polishing of the surfaces.

The inside phenomena were assessed via the photographs of the sectioned impact areas taken with a Canon 6D, equipped with a EF 100 F2.8 lens and flash light, for panels 2, 3, 4 presented on Figures 2, 6, 7 and with a KEYENCE VHX5000 microscope for panel 1 presented on Figure 8. The photographs were taken perpendicularly to the cross-section in order to minimize distortion. Several basic linear distances were measured (Table 4) as shown on Figure 2; they are:

- the exterior deflection and the interior deflection (BFD), that are measured from the front (respectively, back) initial panel planes towards the most advanced parts of the panel as a result of the impact;
- the bullet trace diameter in its narrowest entrance part; its deviation from the bullet calibre is a measure of the panel elastic deformation during penetration;

- the penetration, that can be evaluated either as a thickness of the plies that had been perforated, or their percentage (the direct calculation of number of plies appeared to be laborious, and this value was measured by visually tracing the cavity into the material away from the impact location. The penetration was measured on both sides from the hole, unless the hole approached the edge of the panel, and the two values differed no more than 2%);
- the ‘Initial’ unpenetrated portion of the panel thickness is mathematically deduced as a difference between the initial panel thickness and the ‘penetration’ thickness measurement;
- the ‘final’ unpenetrated portion of the panel thickness is measured along the bullet penetration axis (therefore, ‘final’ is less than ‘initial’ if the panel compaction dominates, and ‘final’ is more than ‘initial’ if the panel delamination dominates).

These values are defined in the meridional plane of the impacts; in reality, the samples after water jet cutting are not planar, both due to significant local unevenness and a global deformation of the section. The linear dimensions are measured on the photographs to achieve better accuracy than direct measurements. The measurements are performed using the *Analysing Digital Images* software. They are independently fulfilled on each of the two sides of the cut, and the difference between them gives the estimate of the neglected asymmetry factors.

For panel 5, the non-pressed layers were easily detached from each other, and the true 3D structure was studied via SEM. We used the SEM machine VEGA II LMU manufactured by TESCAN, equipped with an energy dispersive X-ray microanalysis unit (EDX). The morphostructural studies have been realised at the electron energy of 30 keV; the scannings

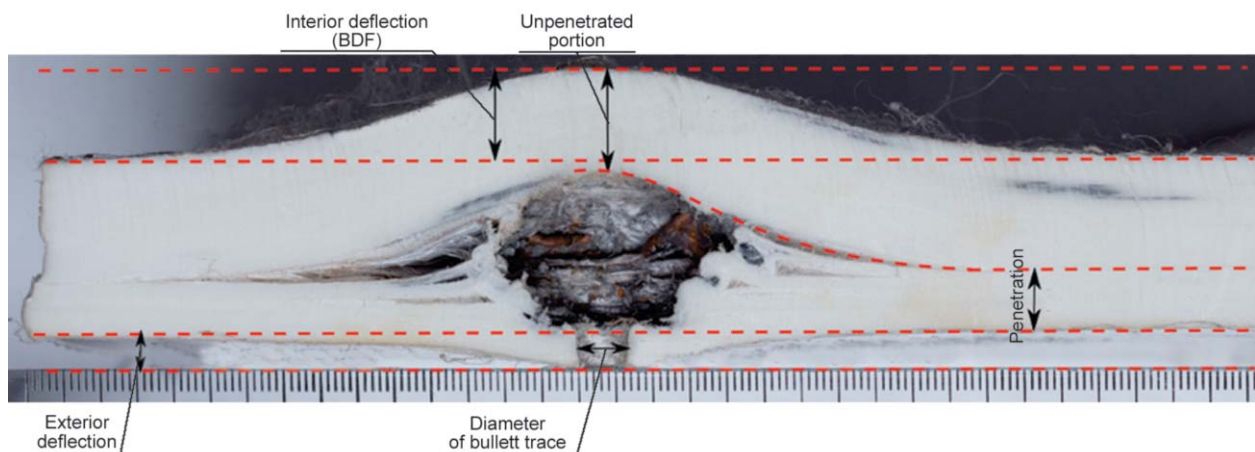


Figure 2. The linear dimensions measured and included in Table 4 (on the example of panel 2).

have been realised at the magnifications ranging from $10\times$ to $1000\times$. On the optoelectronics magnifications that have been used for the morphostructural investigations, the resolution indicated by the machine was around 10 nm. The probes have been investigated in vacuum at a pressure of $4\cdot 10^{-2}$ Pa and ambient temperature. The Bruker AXS EDX unit uses a radiation detector X QUANTAX 4000 and a spectrometer Xflash silicon drift (SD3). The EDX unit also has a discrimination resolution of 125 eV. A Quantax 400 spectrometer with an XFlash 4010 X-ray detector has been used, having a resolution in energy of 125 eV (on Mn-Ka) and Peltier cooling. It can detect and identify chemical elements placed between Be and U (included). However, the EDX performed did not detect any atoms except carbon, and a negligible fraction of oxygen, in the Tensylon[®] tape. The authors, therefore, suppose that the tape constitutes unidirectionally stretched UHMWPE embedded into low density polyethylene (LDPE) matrix with a smaller molecular weight. Alternatively, we can think of UHMWPE unidirectionally stretched filaments being pressed together under elevated temperature, resulting in partial thermal degradation into LDPE, that works as a matrix in the Tensylon[®] tape. This interpretation is consistent with the product description in [17].

3. Results and discussion

As a starting point for comparison of the experimental results, the authors have chosen the two-stage penetration model of [8, 9] for thick UHMWPE.

The first stage, called ‘shear plugging’, is controlled by the fibres (for Dyneema[®]; in Tensylon[®] it is equivalent to fibrils and strips) fracture in shear (in the plane comprising fibrils and the bullet penetration axis) on the perimeter of the penetrating bullet. However, as [8] admits and the authors agree, no direct testing to evaluate shear fracture in this plane has been successful thus far. Indeed, the shear compliance and shear failure actually measured in [18, 19] using the 45° tension set-up is the shear in the plane containing the fibres. The one measured in [20] is the inter-laminar shear. [21] implemented both of these methods. In the former case, it was measured perpendicularly to the bullet penetration axis; in the latter, failure in inter-laminar shear cannot be considered as a primary failure mechanism as it does not

produce a perforation. [22], in a single-support beam series of experiments, and [23], in a double-support beam series of experiments, did not succeed in observing failure: instead, large, evidently, geometrically non-linear shear deformations occurred.

In [8], an indirect method of the shear strength estimation was proposed. It relates it to the tensile strength of the fibres, and was verified on the epoxy-filled Kevlar[®] fibres composites. Another physical interpretation of the fibre failure in the first stage is possible, that does not require the material shear strength. It directly relates fibre failure to their longitudinal failure. In UHMWPE composites with highly plastically deformable matrices like polyurethane (in Dyneema[®] HB26) or LDPE in the material of interest, the limit of the fibre rotation is usually not achievable. However, under high strain rate loading fibres do not necessarily get the V-shape as assumed in the Cunniff description [5]. If the shear speed of sound that puts the panel front face into motion along the penetrating bullet is not high enough compared to the bullet penetration speed, the strips tend to be U-shape deformed, with the significant strain concentration around the vicinity of the projectile side surface (Figure 3). These considerations give a slightly different insight in the formula proposed in [8].

The second stage, called ‘bulging’, is, in some sense, a replica of the thin UHMWPE ballistic response, i.e. it considers that the whole panel deforms as a membrane until (unluckily) it is perforated all-at-once if the material rupture tensile strain is reached. The assessment of the panels’ response begins in paragraph 3.1 by describing the behaviour of the non pressed panel 5. As already mentioned, this panel was tested because its internal structure could be easily visualised and studied with a microscope and SEM. The penetration mechanisms observed are used as a basis for the real protective solutions response analysis in paragraph 3.2.

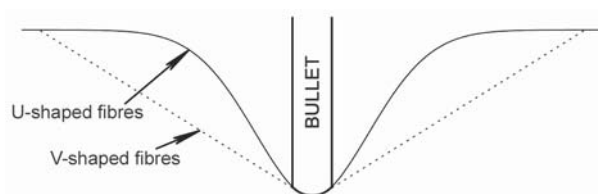


Figure 3. The V-shape of yarns under transversal impact in the model of Cunniff [5] compared to a more realistic U-shape that takes the wave attenuation into account.

3.1. Non-pressed Tensylon® panel ballistic response

The overall post-mortem view of the non-pressed panel 5 is shown on Figure 4. The panel suffered a full penetration without a global BFD. Apart from the first and the last layers (that severely delaminated), all the other layers behaved similarly. According to the theory of [8], as well as [15], ballistic performance is driven by tension for thin panels, and for thick panels at least on the second stage of penetration. The theory, therefore, predicts that significant bulging should occur, and that the ballistic performance should only slightly vary with the panel pressing. However, the residual bulge deformation was not evidenced, and the ballistic resistance was significantly inferior. The diamond shape that formed around the bullet hole (Figure 4) shows that the material is severely damaged at least two calibres away from the perforation along the directions of the fibres, while no damage is visible in the diagonal directions.

The difference between theoretical predictions and our observations can be attributed to the crucial role of the speed of sound in Tensylon®, and especially to the shear speed of sound. Its role was already discussed in [6]. In the case of a bunch of fibres studied by Cunniff [5], the shear speed of sound degenerates into a string speed of sound. This value is proportional to the square root of the tensile force and inversely proportional to its linear density, i.e. it is no longer a material characteristic, and since the fibres are not pretensioned in the non-pressed setup, the speed of sound in the lateral direction is very low. In the case

of a hard ballistic panel, the shear speed of sound in the panel is relatively high, yet less than the longitudinal speed of sound. At the early stage of penetration, the laterally propagating wave quickly decays with the distance travelled, as it is dispersed in a 3D surrounding (in comparison to propagation along a 1D yarn in Cunniff's setting). The strip deformation takes the form of a U-shape, with failure in the strain (and, apparently, stress) concentration zone.

The transition from a 3D wave dispersion into a 2D wave dispersion can be associated with the shock (or sound) wave propagation towards the back face of the panel and its return as a rarefaction wave to the bullet tip. As a result, the whole panel in front of the projectile is put into motion, and the shear stresses/local deformations in it decrease substantially. This transition, related to the second stage of penetration initiation, is characterised by the membrane-type response of the panel. The strips of material become less bent near the edges of the projectile, and can provide longer (in a sense of both distance, that corresponds to the increase of work done, and time, that corresponds to the increase of momentum transferred) contact with the bullet before failure. In an idealized setting, a membrane is perforated all-at-once; thermal load and friction provide partial perforation on the second stage.

In this understanding, we can interpret the failure of a set of ply-precursor tapes stretched. Because of the multiple interfaces and occasional voids in the non-pressed setting, the longitudinal sound speed in the direction of bullet penetration significantly decays,

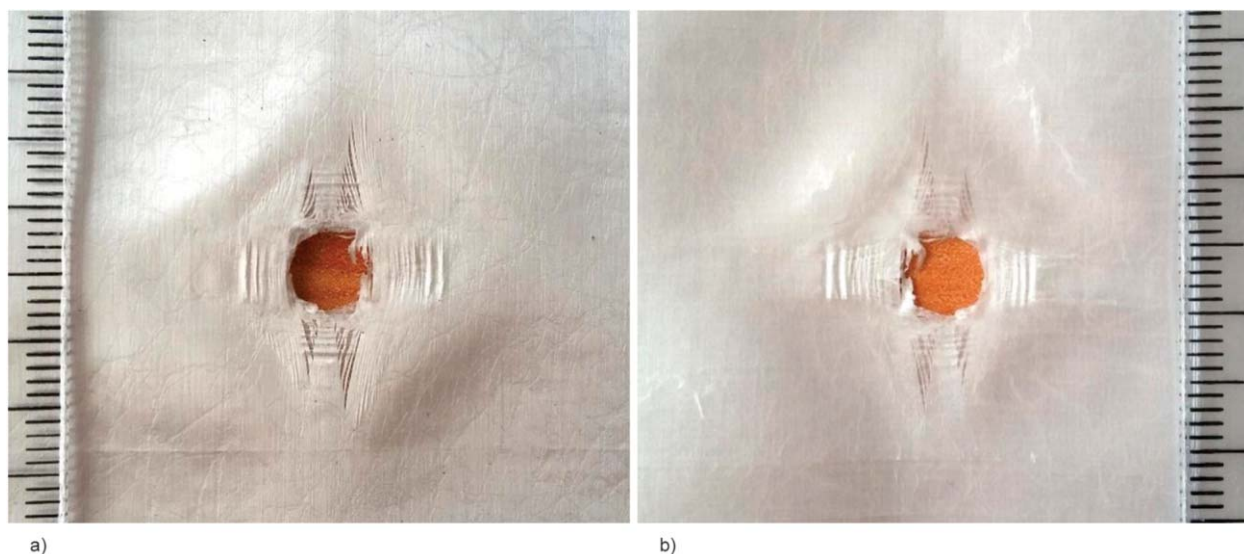


Figure 4. Post-mortem view of one layer (two plies) of Tensylon® tape arbitrarily taken from inside the unpressed panel 5, perforated by a bullet. a) front view (the 'entrance' of the bullet); b) back view (the exit of the bullet).

and shear deformations do not propagate at all. As a consequence, the reflection from the back face is severely weakened and the back-and-forth time approaches the bullet penetration time. On the other hand, a set of backing tapes is significant enough to dampen the V-shape permanent deformation of the front tape. The result is the U-type failure of each tape, drastically reducing the ballistic protection efficiency. This reduction has similar origins as the reduction from Kevlar® 29/resin composite panel versus dry Kevlar® 29 fabric presented in [6]: the polymer matrix plays the same role as the panel compaction for Tensylon®. It is expected, although not based on enough experimental evidence due to insufficient number of tests, that V_{50} for the ply-precursor tape follows the thin-panel analytical prediction like the one proposed in [6]. We can also interpret the experimental result in a sense of [19]: absence of shear strength in a set of Tensylon® tapes is a factor significantly reducing its ballistic protection capability.

The in-ply failure along the principle direction (i.e., along the fibril direction, so that no fibrils get ruptured) is clearly visible on Figure 4. It suggests that the ply was subjected to tension perpendicular to the principle direction or to in-ply shear. The strips met by the bullet tip have failed, whereas on the sides of the projectile, they were pushed out, and torn from each other. This effect is better seen on the SEM images on Figure 5.

The typical element of the SEM images is the strips of material, that can go as small as $62\text{ }\mu\text{m}$ and as large as $301\text{ }\mu\text{m}$ (Figure 5d). These strips often have characteristic longitudinal structure (as if the strips were about to split into several narrower strips) and slightly inclined perpendicular structure. These latter features correspond to strips buckling (both in-plane and out-of-plane folding, Figure 4), and are confined to the parts where they are bent. These features can also be viewed as a sign of the kinking domains, that occur in fibres and other unidirectionally stretched

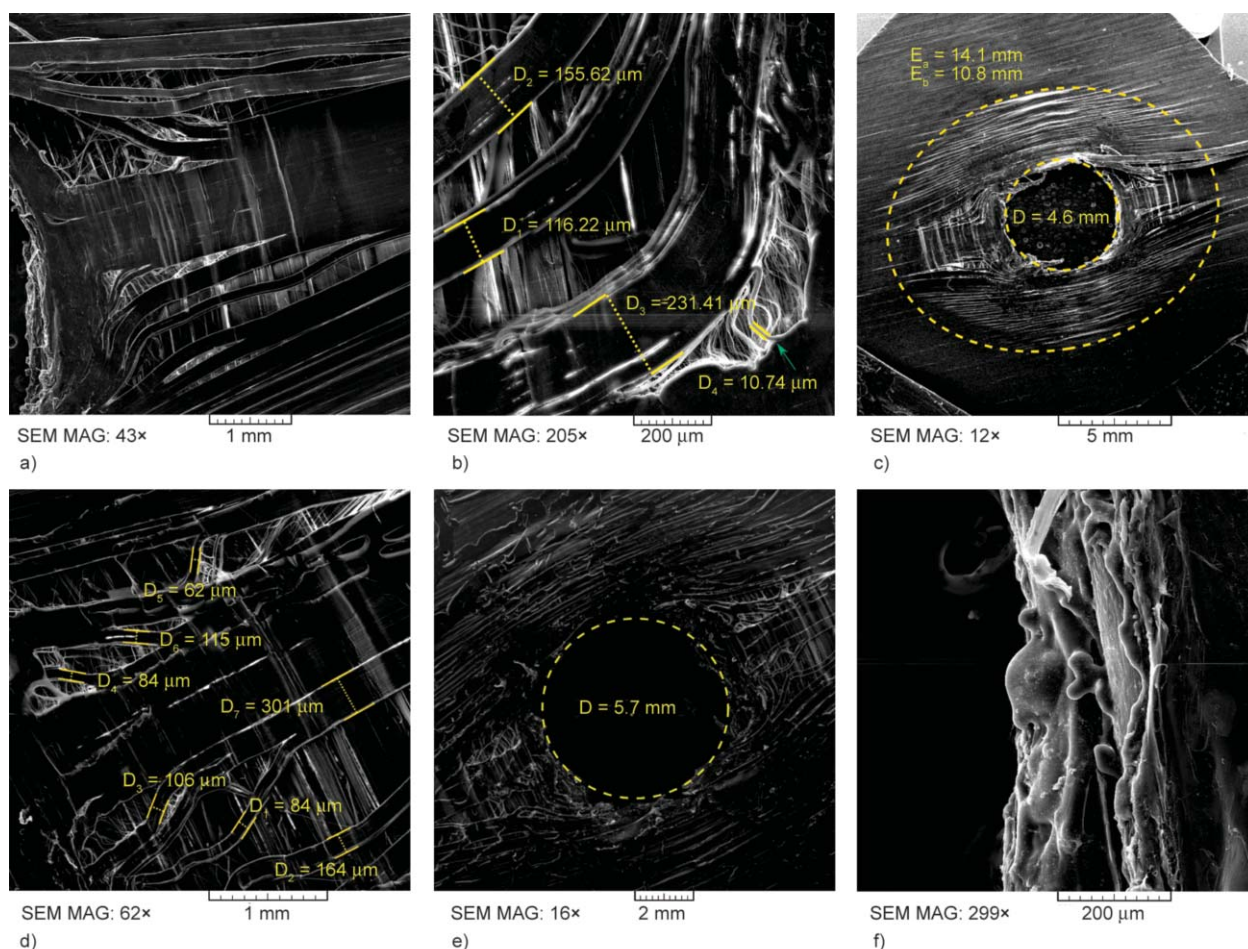


Figure 5. SEM images of the interior perforated Tensylon® ply-precursor tape. (a)–(c), (f) first impact; (d)–(e) second impact. (c), (e) overall view of the holes; (a), (d) detailed appearance of the 'strips'; (b) width of 'strips'; (f) the vicinity of the perforation close inspection.

materials under compression failure, both quasi-static and dynamic [24].

SEM images do not provide the 3D shape of these ‘elements’. However, it can be reconstructed: in-between the strips, visible on the images at moderate magnification ($30\times$ – $200\times$) like on Figures 5a, 5d, the underneath ply is visible. Therefore, the strips must be having the thickness of the ply. At higher magnification (Figure 5b and especially 5f), the material irregularities become clearly visible. These irregularities occur in the domain subjected to friction with the bullet and subsequent heating. The 1D orientation of molecules obtained during solid-state extrusion is destroyed, and curvilinear shapes occur.

Neither SEM, nor optical microscopy (KEYENCE) allowed the visualisation of individual fibres, as it happens on similar products like Dyneema® HB 26. This is the reason why the term ‘fibre’ regarding Tensylon® is avoided; instead, the terms like ‘ply’, ‘sheet’ for a unidirectional entity, and ‘strip’ for a fraction of a sheet of 50–300 μm width (and, supposingly, around 60 μm thickness) are more appropriate.

Figure 5a clearly shows three types of unidirectional ply responses, as a function of the distance to the impact center:

- the central part was, supposingly, perforated at the very instant of impact, and therefore no tension wave propagation signs are visible;
- the periphery region was first subjected to tension wave propagation, which resulted in both interply delamination and in-ply splitting, and then the strip rupture resulted in the two debris fractions gaining both longitudinal and lateral momentum;
- the further part of the ply was not subjected to failure and, as a consequence, has been under tension for the longest time. It results in the longest delamination path, and the largest out-of-plane displacement. The latter can be associated with the influence of friction between the penetrating bullet and the panel.

It is interesting to mention that the penetration hole diameter varies significantly from strike to strike: the values 4.6 and 5.7 mm have been measured for strikes 1 (Figure 5c) and 2 (Figure 5e), respectively. This large discrepancy suggests that the hole diameter in post-mortem analysis is not a characteristic parameter of the perforation process.

The hole observed post-mortem reaches its final state after the penetrating bullet has passed away, i.e., behind its rear edge. The hole is formed by the four

strips that used to be in contact with the projectile during penetration, but after the passing of the bullet these respective strips could have displaced back (towards the impact hole). It is worth pointing out that the strips are not bonded together (the whole vicinity of the perforation is delaminated, and so 0 and 90° strips could freely move relative to each other during the impact). The strips were subject to tension and to friction-associated heating (due to their nearly tangential orientation, the corresponding stress in the bullet was significantly lower, and the bullet deformations were low). The final position of the strips is primarily governed by (a) its plastic elongation (that, as shown in tape tension experiments [25], occurs at low stresses, and therefore cannot be used to estimate the maximum stress reached in the dynamic loading) and (b) the length of the delaminated part of the strip. Both these values are subject to variation, since the material is not uniform, and the respective characteristics are not averaged in volume.

3.2. Hard Tensylon® panels ballistic response

None of the hard ballistic panels tested (presented in Table 2) got perforated in our series of ballistic experiments. As presented in Table 4, residual compressive strain was observed in front of the bullet in the hard ballistic panel impacted both separately and with a backing steel sheet, with the exception of the impact in the vicinity of the edge. This latter case resulted in the impact cavity stretching until the panel edge (68 mm, or 9 calibres, away) and extending there, and the rarefaction wave reflected from the free side wall has led to the panel delamination, increasing the thickness. In the remaining cases, the residual compression is a sign of high stresses generated by the bullet throughout the panel thickness, that has propagated in a shock compression wave.

The BFD was observed in panels 2–4. As expected, the BFD was significantly inferior both in the shielded panel 3 and the backed panel 4. For the sandwiched panel 1, the BFD was too small to be measured, and, at the same time, the delamination was much more pronounced. The measurements of the panel final thickness were, therefore, prohibitively inaccurate, and the penetration percentage was ~15%. It should be noted that in presence of the backing steel sheet the perforated portion of the composite plate was ~4 % bigger than for the UHMWPE panel without protection. This fact is in agreement with the concept of the sound wave back-and-forth passage

Table 4. Basic linear dimensions of the partially penetrated holes in a ‘bare’ Tensylon® panel (panel 2), a Tensylon® panel with steel shield (panel 3) and backing (panel 4).

	Side	Exterior deflection [mm]	Interior deflection [mm]	Diameter of bullet trace [mm]	Penetration [%]	Dimensions of the unpenetrated portion [mm]	
						Initial	Final
Panel 2 Shot 1	1	5.2	12.1	6.2	36.4	14.3	14.4
	2	4.6	12.7	7.2	33.8	14.9	14.3
Panel 2 Shot 2	1	4.9	13.7	7.2	36.9	14.2	15.1
	2	4.5	13.8	7.2	36.4	14.3	15.2
Panel 3 Shot 1	1	–	4.3	–	10.1	21.1	20.7
	2	–	4.6	–	10.2	21.1	20.8
Panel 3 Shot 2	1	–	4.2	–	8.7	21.0	20.7
	2	–	4.1	–	9.9	21.0	20.8
Panel 4 Shot 1	1	5.1	5.0	6.5	40.9	13.3	12.9
	2	4.7	5.2	6.5	39.1	13.7	12.9
Panel 4 Shot 2	1	4.8	4.9	7.1	41.3	13.2	13.2
	2	4.4	4.7	7.3	35.6	14.5	13.5

as a prerequisite for the ‘shear plugging’ stage termination, and the ‘bulging’ stage initiation. However, a number of peculiarities should be stated:

- the bullet-induced perforation is square rather than circular. Therefore, it seems reasonable to use the perforation hole perimeter, rather than the bullet perimeter, to estimate the momentum and energy transferred from the bullet to the panel;
- the size of the perforation is smaller than the calibre. By analogy with the panel 5 response, supposingly, all the plies had been delaminated in the vicinity of the impact, and the strips bordering the postmortem hole had reversibly displaced to the bullet external diameter of 8.03 mm.

The role of the front steel sheet in experiments 1 and 3 (2.5, respectively 3.0 mm) can be interpreted as follows. Its major role in the setting is to provide a shear wave propagation mechanism (as 3 mm of steel possess a significant bending stiffness). The compression wave in Tensylon® propagates in a quasi-1D mode in this case, with the primary direction along the projectile, with a decaying amplitude related to the axisymmetric wave in the front steel sheet. As a result, the whole Tensylon® plate is put into motion from the very beginning, resulting in the ‘bulging’ stage of Tensylon® response. If the front steel sheet does not get perforated (experiment 3), the expected predominant failure mechanism that remains active under such loading is the heating: propagation of compression waves, and different Poisson ratios of steel and Tensylon® leading to relative friction of the two materials lead to melting of matrix and damaging of fibrils. However, these processes accumulate

a significant portion of the bullet’s energy. If it gets perforated (experiment 1), the effective penetrating mass increases on the mass of the steel fragments, while the effective penetrating velocity decreases due to various reasons associated with the longitudinal and transversal shock wave effects prior to the projectile penetration into the UHMWPE. The percentage of the penetrated layers decreased substantially, even though the backing sheet was present. Photographic analysis of the impacted panels cross-sections (Figures 6–8) reveals approximately the same failure patterns as reported previously in [3, 4]. The narrow part of the bullet channel is filled with the black dots, characteristic of UHMWPE thermal degradation. Hine *et al.* [17] distinguishes two temperature ranges that lead to degradation, and the corresponding mechanisms. At about 132 °C, a small fraction of material, that was melted and recrystallized during the hard panel pressing, melts. Slightly above 150 °C, the whole unidirectionally stretched crystalline phase melts. Such high temperature could have been reached by compression shock wave heating in combination with friction with the bullet side. We do not have a comparison of the role of these two sources of heating. However, we can roughly estimate the shock wave heating as follows. We will assume the shock wave compression described by the shock equation of state. In addition, we will assume 1D wave propagation, and use the data [8, 26] on Dyneema® HB26 for Tensylon®: $u_s = 3.57 + 1.3u_p$, where both the shock wave u_s and the particle u_p velocities are in [km/s], and $\rho = 0.98 \text{ g/cm}^3$. The lead-core bullet consists of two metals, with the biggest fraction of

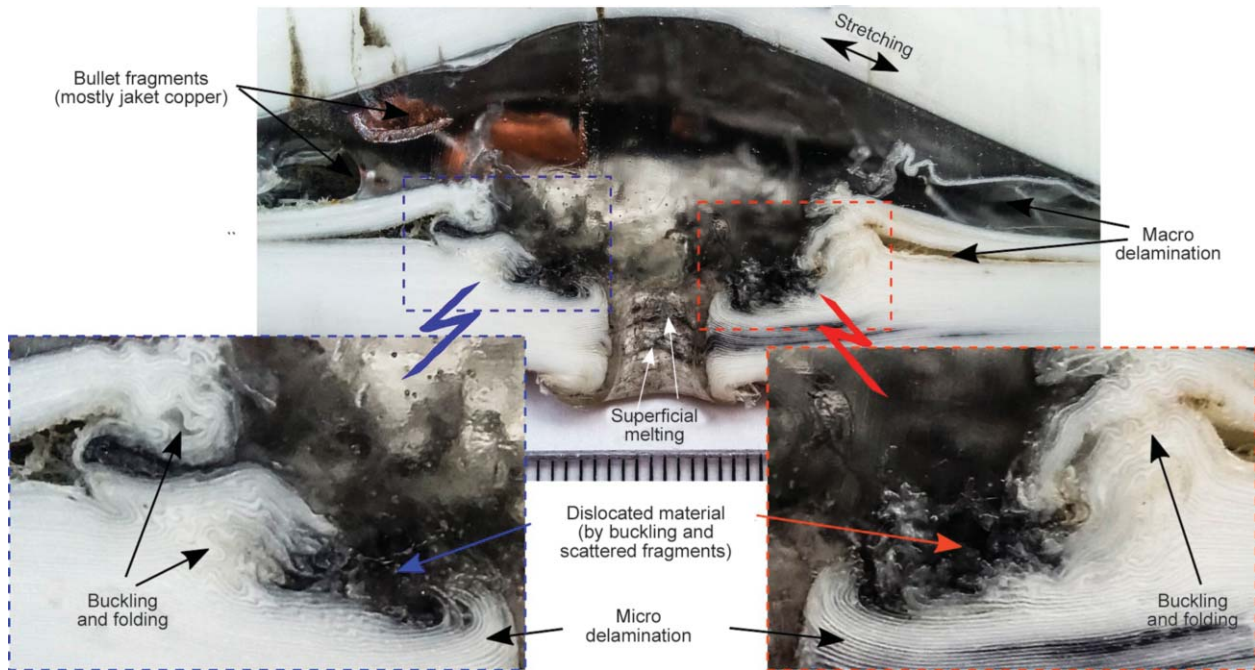


Figure 6. The cross-section of the impact into panel 2 (without protection).

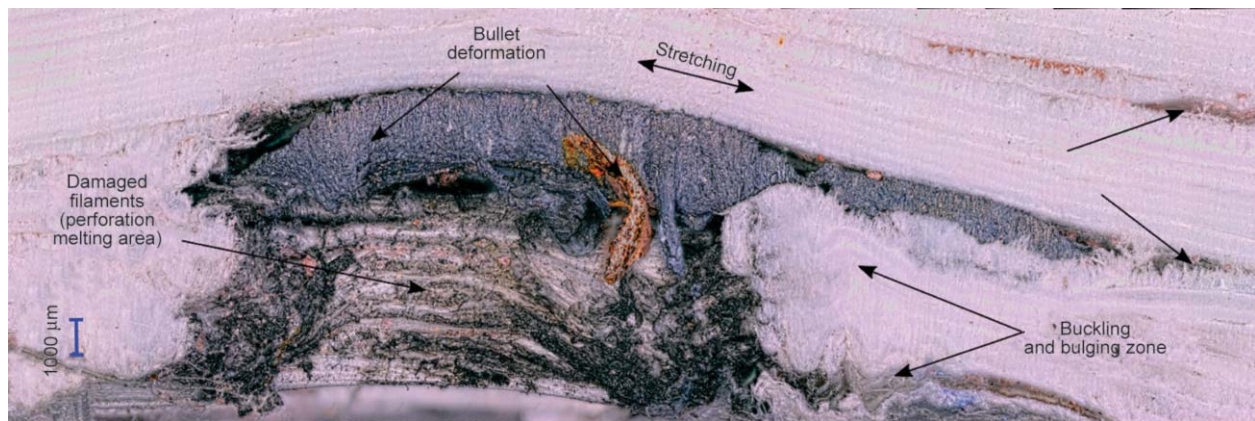


Figure 7. The cross-section of the impact into the sandwiched panel 1, KEYENCE VHX-5000 microscope.

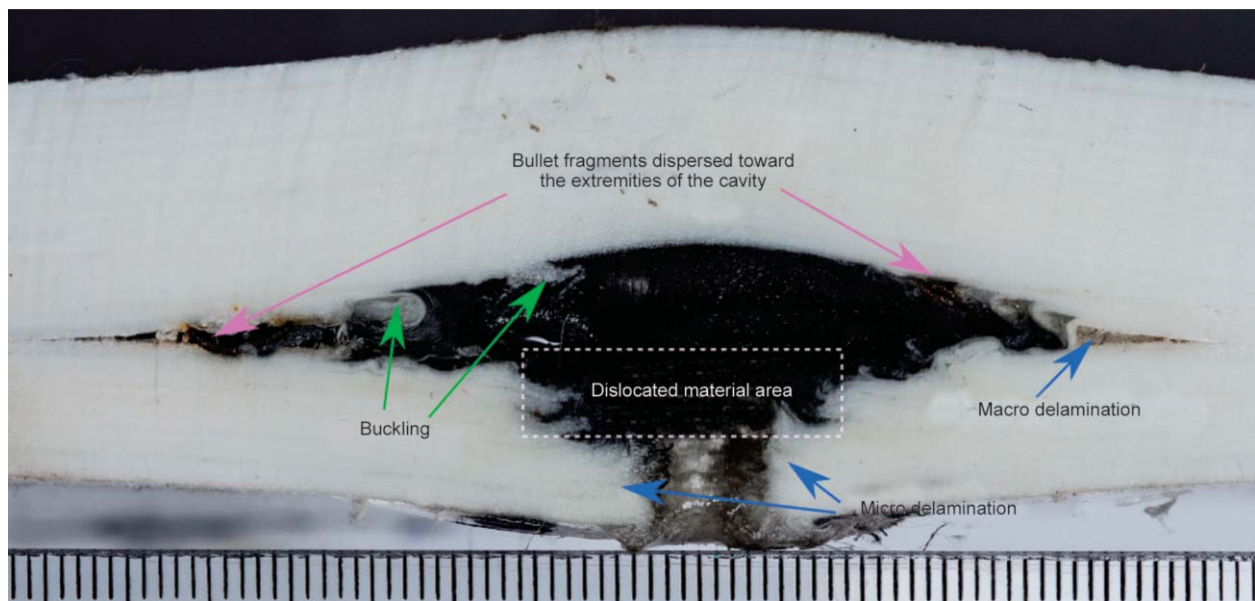


Figure 8. The cross-section of the impact into the backed panel 4, Canon 6D camera.

lead; therefore, we used its data from [27]: $u_s = 2.006 + 1.538u_p$, $\rho = 11.34 \text{ g/cm}^3$. With the shock polar technique, we can obtain that the PE density rises to $\rho_1 = 1.14 \text{ g/cm}^3$ under an impact at 700 m/s. The simplest way to estimate temperature rise is by assuming the UHMWPE heat capacity constant with temperature and specific volume: using the value $C_v = 1.85 \text{ kJ/kg/K}$ [8, 26], we get $\Delta T_1 = 96^\circ\text{C}$ (for $T_i = 20^\circ\text{C}$ in the initial state of the panel). The more accurate approach of [28] requires, in addition, the Grüneisen coefficient γ . Assuming it specific volume independent and equal to $\gamma_0 = 1.64$ [8, 26], we arrive at the post-shock temperature of $T_{12} = 112^\circ\text{C}$, $\Delta T_2 = 92^\circ\text{C}$ respectively, i.e. 4°C lower. These values are close to, but bellow the melting temperature for Tensylon®. The edge effects and the reflected release waves decrease the panel temperature, whereas friction gives another mechanism for its growth.

The strips of material in panels 1, 2, 4 around the cavity are significantly buckled in a way similar to the one being observed on non-pressed panel 5, but in this case these curved strips are additionally created by the debris ricocheting in the cavities in all directions. The copper bullet jacket has remained in the form of big fragments, whereas the lead core approached a typical mushroomed shape in panel 1 (Figure 7) and was most probably sprayed inside the cavities of panels 2 and 4 (Figures 6 and 8). The stretched material in front of the cavity is also clearly visible.

The internal view of the cavity is minorly influenced by the backing, that can be confirmed by comparison of Figures 6, 7 and 8 obtained under different shooting conditions. The shielded panel (Figure 9), on the contrary, has no cavity at all: the shielding sheet was

severely deformed, but was not perforated. As a result, the impact on the Tensylon® plate was spread on a significantly wider area, associated with only a 10% penetration, and accompanied with intense thermal degradation through heating (unlike the other cases, where only black points were visible, the whole vicinity of the impact became black).

4. Conclusions

A set of experimental shootings into Tensylon® ballistic protection panels with Kalashnikov 7.62×39 mm FMJ/MC ammunition has been performed. The panels were studied postmortem using photography, optical microscopy and SEM. Non-pressed panels performance was compared with the hard panels performance under identical test conditions. Having the same tensile strength and longitudinal strain to failure, these two types of panels substantially differ in their bending stiffness. Consistent with the [8] approach, higher bending stiffness is associated with enhanced ballistic performance. Experiments show that bending stiffness is responsible for the regime of the bullet penetration: either a ballistic-protection effective ‘bulging’, or a far less efficient ‘shear plugging’ regime. Additional bending stiffness associated with a steel sheet used in a stratified protective solution is especially effective if implemented in order to increase the front portion bending stiffness.

However, at least two problems are associated with single-material hot-pressed Tensylon® hard protective panels for personal armour. Firstly, they significantly obstruct (due to their bending stiffness) the motion of the personnel (suppositionally, it is even more unpleasant than the weight penalty associated with the panel). Secondly, it improves protection against

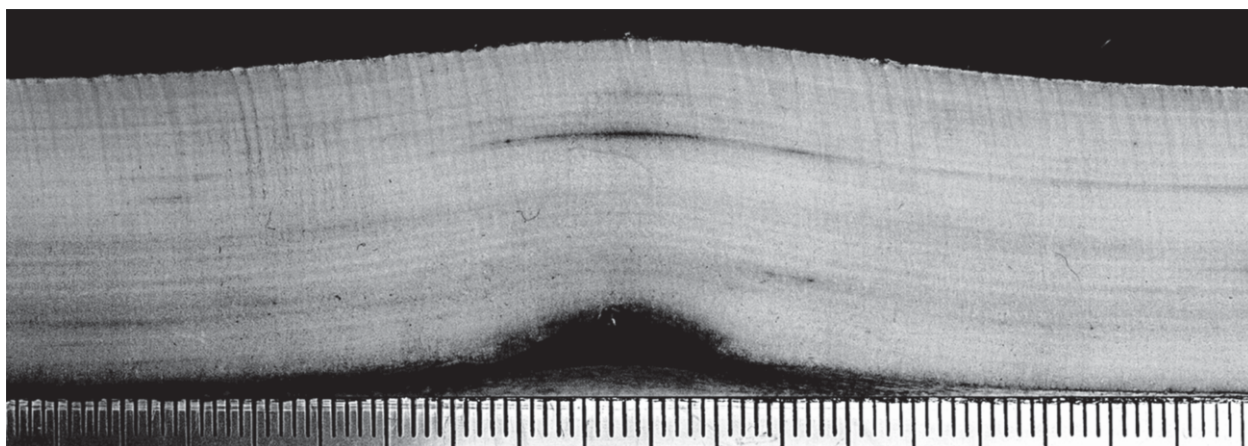


Figure 9. The cross-section of the impact into the shielded panel 3 (the image is under-exposed and the contrast is increased).

perforation, i.e. V_{50} , on the cost of increasing (or, at least, without improvement) the BFD, i.e. the blunt trauma.

The experiments fulfilled on hard ballistic panels did not allow to obtain the V_{50} value, since 2/3 of the panel thickness was not perforated in all tests, and the BFD was also three times lower than the maximum admissible by the standard. On the other hand, it is known [28] that the perforated portion of the ballistic panels increases drastically with the increase of velocity, so that the V_{50} velocity is not more than 20–30% underestimated.

Acknowledgements

The authors are thankful for the support offered by: STIM-PEX company (who provided the necessary materials), Thomas Bonnemains, IUT Brest (who helped with the waterjet cutting), prof. Lorena Deleanu, UGAL Galati (who suggested a lot of improvement ideas for the final version of this article) and project ‘IED PROTECT’ – Modular composite structures for protection against complex effects of improvised explosive devices, National Program ‘Partnerships in prioritized areas PN II’, contract no. 283/2014.

References

- [1] Frissen R. J. T.: Modelling the ballistic impact behaviour of polyethylene-fibre-reinforced composites. Stan Ackeprnans Institiliit, Eindhoven (1996).
- [2] Jacobs M. J. N., van Dingenen J. L. J.: Ballistic protection mechanisms in personal armour. *Journal of Materials Science*, **36**, 3137–3142 (2001).
<https://doi.org/10.1023/a:1017922000090>
- [3] O’Masta M. R., Deshpande V. S., Wadley H. N. G.: Mechanisms of projectile penetration in Dyneema® encapsulated aluminum structures. *International Journal of Impact Engineering*, **74**, 16–35 (2014).
<https://doi.org/10.1016/j.ijimpeng.2014.02.002>
- [4] O’Masta M. R., Crayton D., Deshpande V. S., Wadley H. N. G.: Mechanisms of penetration in polyethylene reinforced cross-ply laminates. *International Journal of Impact Engineering*, **86**, 249–264 (2015).
<https://doi.org/10.1016/j.ijimpeng.2015.08.012>
- [5] Cunniff P. M.: Dimensionless parameters for optimization of textile based body armor systems. in ‘Proceedings of the 18th International Symposium of Ballistics’ San Antonio, USA, 1303–1310 (1999).
- [6] Walker J. D.: Ballistic limit of fabrics with resin. in ‘19th International Symposium on Ballistics, Interlaken, Switzerland’ 1409–1414 (2001).
- [7] Wilhelm M., Bir C.: Injuries to law enforcement officers: The backface signature injury. *Forensic Science International*, **174**, 6–11 (2008).
<https://doi.org/10.1016/j.forsciint.2007.02.028>
- [8] Nguyen L. H.: The ballistic performance of thick ultra high molecular weight polyethylene composite. PhD thesis, School of Engineering, College of Science Engineering and Health, RMIT University (2015).
- [9] Nguyen L. H., Ryan S., Cimpoeru S. J., Mouritz A. P., Orifici A. C.: The effect of target thickness on the ballistic performance of ultra high molecular weight polyethylene composite. *International Journal of Impact Engineering*, **75**, 174–183 (2015).
<https://doi.org/10.1016/j.ijimpeng.2014.07.008>
- [10] Meshi I., Amarilio I., Benes D., Haj-Ali R.: Delamination behavior of UHMWPE soft layered composites. *Composites Part B: Engineering*, **98**, 166–175 (2016).
<https://doi.org/10.1016/j.compositesb.2016.05.027>
- [11] Haight C., McNamara K., Courtney M.: Does V_{50} depend on armor mass? USAF Academy, Fairchild Drive (2012).
- [12] Ballistic resistant protective materials. Technical Report 0108.01, National Institute of Justice (1985).
- [13] Ballistic resistance of body armor. Technical Report 0101.06, National Institute of Justice (2008).
- [14] Carbajal L., Jovicic J., Kuhlmann H.: Assault rifle bullet-experimental characterization and computer (FE) modeling. in ‘Experimental and applied mechanics’ (ed.: Proulx T.) Vol 6, 651–668 (2011).
https://doi.org/10.1007/978-1-4614-0222-0_77
- [15] Phoenix S. L., Porwal P. K.: A new membrane model for the ballistic impact response and V_{50} performance of multi-ply fibrous systems. *International Journal of Solids and Structures*, **40**, 6723–6765 (2003).
[https://doi.org/10.1016/S0020-7683\(03\)00329-9](https://doi.org/10.1016/S0020-7683(03)00329-9)
- [16] Utomo B. D. H.: High-speed impact modelling and testing of Dyneema composite. PhD thesis, Technische Universiteit Delft (2011).
- [17] Hine P. J., Ward I. M., Jordan N. D., Olley R. H., Bassett D. C.: A comparison of the hot-compaction behavior of oriented, high-modulus, polyethylene fibers and tapes. *Journal of Macromolecular Science Part B: Physics*, **40**, 959–989 (2001).
<https://doi.org/10.1081/MB-100107570>
- [18] Iannucci L., Pope D.: High velocity impact and armour design. *Express Polymer Letters*, **5**, 262–272 (2011).
<https://doi.org/10.3144/expresspolymlett.2011.26>
- [19] Russell B., Karthikeyan K., Deshpande V. S., Fleck N.: The high strain rate response of ultra high molecular-weight polyethylene: From fibre to laminate. *International Journal of Impact Engineering*, **60**, 1–9 (2013).
<https://doi.org/10.1016/j.ijimpeng.2013.03.010>
- [20] O’Masta M. R., Deshpande V. S., Wadley H. N. G.: Defect controlled transverse compressive strength of polyethylene fiber laminates. *International Journal of Solids and Structures*, **52**, 130–149 (2015).
<https://doi.org/10.1016/j.jisolsolstr.2014.09.023>
- [21] Karthikeyan K., Russell B., Fleck N., Wadley H. N. G., Deshpande V. S.: The effect of shear strength on the ballistic response of laminated composite plates. *European Journal of Mechanics Part A: Solids*, **42**, 35–53 (2013).
<https://doi.org/10.1016/j.euromechsol.2013.04.002>

- [22] Liu G., Thouless M., Deshpande V. S., Fleck N. A.: Collapse of a composite beam made from ultra high molecular-weight polyethylene fibres. *Journal of the Mechanics and Physics of Solids*, **63**, 320–335 (2014).
<https://doi.org/10.1016/j.jmps.2013.08.021>
- [23] Lässig T., Nguyen L., May M., Riedel W., Heisserer U., van der Werff H., Hiermaier S.: A non-linear orthotropic hydrocode model for ultra-high molecular weight polyethylene in impact simulations. *International Journal of Impact Engineering*, **75**, 110–122 (2015).
<https://doi.org/10.1016/j.ijimpeng.2014.07.004>
- [24] Attwood J., Fleck N., Wadley H., Deshpande V.: The compressive response of ultra-high molecular weight polyethylene fibres and composites. *International Journal of Solids and Structures*, **71**, 141–155 (2015).
<https://doi.org/10.1016/j.ijsolstr.2015.06.015>
- [25] Alil L., Arrigoni M., Badea S., Barbu C., Istrate M., Mostovyykh P.: On the constitutive law for the mechanical quasi-static response of criss-cross composites (on the example of UHMWPE). *Human Factors and Mechanical Engineering for Defense and Safety*, **1**, 4/1–4/12 (2017).
<https://doi.org/10.1007/s41314-017-0006-5>
- [26] Nguyen L. H., Lässig T. R., Ryan S., Riedel W., Mouritz A. P., Orifici A. C.: Numerical modelling of ultra-high molecular weight polyethylene composite under impact loading. *Procedia Engineering*, **103**, 436–443 (2015).
<https://doi.org/10.1016/j.proeng.2015.04.043>
- [27] van Thiel M., Shaner J., Salinas E.: Compendium of shock wave data. Volume 1. Revision 1. Introduction. Section A1-Elements. Lawrence Livermore Laboratory, Livermore (1977).
- [28] Attwood J., Russell B., Wadley H., Deshpande V.: Mechanisms of the penetration of ultra-high molecular weight polyethylene composite beams. *International Journal of Impact Engineering*, **93**, 153–165 (2016).
<https://doi.org/10.1016/j.ijimpeng.2016.02.010>